Electronic Supplementary Material (ESI) for Dalton Transactions

Introducing a photo switchable azo-functionality inside Cr-MIL-101-NH_2 by covalent post-synthetic modification

Antje Modrow[a], Dordaneh Zargarani[b], Rainer Herges[b] and Norbert Stock[a]

[a]Institut für Anorganische Chemie, Christian-Albrechts-Universität, Max-Eyth-Straße 2, D-24118 Kiel (Germany)

Fax: (+49) 0431-880-1775

E-mail: stock@ac.uni-kiel.de

[b]Otto-Diels-Institut für Organische Chemie, Christian-Albrechts-Universität, Otto-Hahn-Platz 4, D-24098 Kiel (Germany)

(1) XRPD-pattern of Cr-MIL-101-NO_2 and Cr-MIL-101-NH_2

The theoretical powder pattern of Cr-MIL-101 (Figure S1, black graph) agrees well with the measured powder pattern of Cr-MIL-101-NO_2 (Figure S1, green graph) and Cr-MIL-101-NH_2 (red graph). No further reflections were observed; therefore no other crystalline phase is present in the samples.

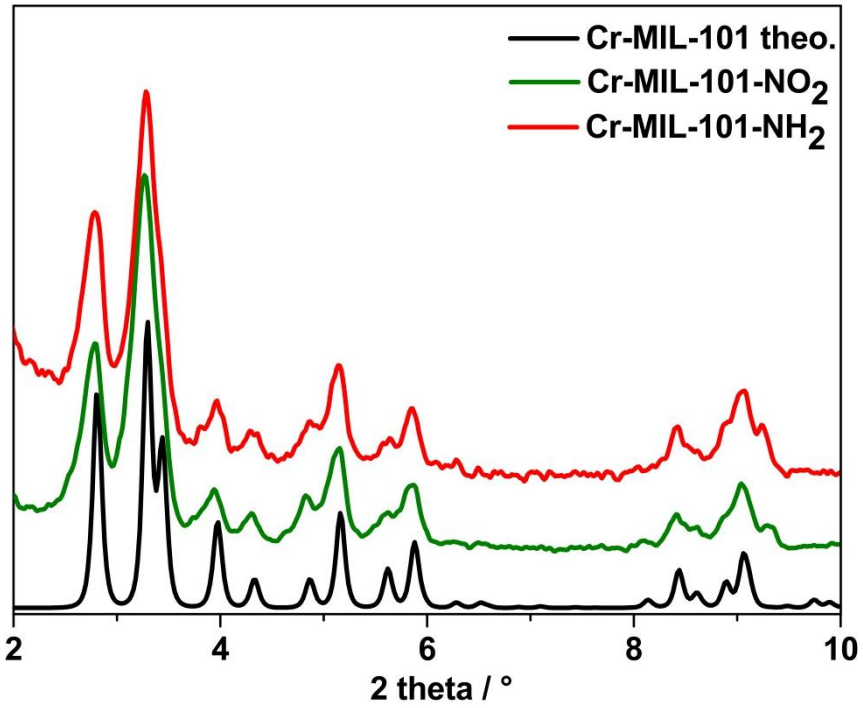

Fig. S1. XRPD pattern of Cr-MIL-101: theoretical pattern (black graph), measured powder pattern of Cr-MIL-101-NO_2 (green graph) and measured powder pattern of Cr-MIL-101-NH_2 (red graph).

(2) IR spectra of Cr-MIL-101-NO_2 and Cr-MIL-101-NH_2

The IR spectra of Cr-MIL-101-NO_2 and Cr-MIL-101-NH_2 are shown in figure S2a and S2b, respectively. The NH_2 (3486 and 3366 cm^{-1}) and the –C-N stretching vibrations (1338 and 1256 cm^{-1}) are clearly visible in the IR spectra of Cr-MIL-101-NH_2 (S2b) compared to the IR spectrum of Cr-MIL-101-NO_2. In this spectrum one can find the asymmetric –NO_2 stretching vibration at 1542 $cm^{-1.}$

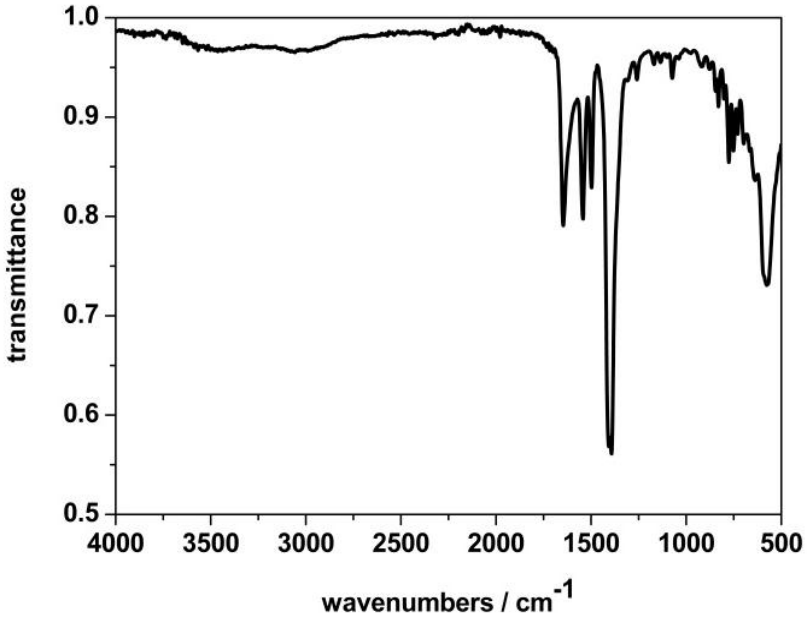

Fig. S2a: IR spectrum of Cr-MIL-101-NO_2

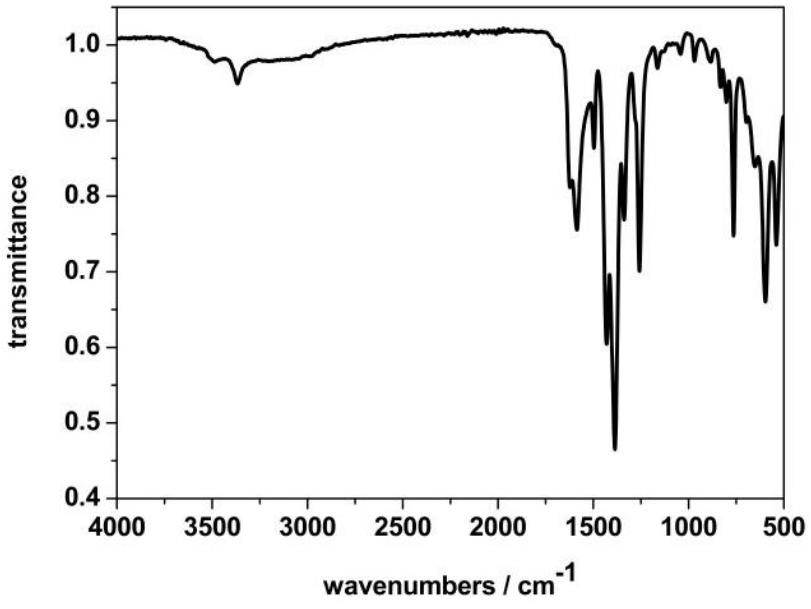

Fig. S2b: IR spectrum of Cr-MIL-101-NH_2

(3) N_2 adsorption isotherm of Cr-MIL-101-NO_2 and Cr-MIL-101-NH_2

In Figure S3 the N_2 sorption isotherms of Cr-MIL-101-NO_2 (filled and open squares) and Cr-MIL-101-NH_2 (filled and open cycles) are shown. The specific surface area was calculated from the Brunauer-Emmett-Teller (BET) plot using the approach introduced by Rouquerol et al.. For Cr-MIL-101-NO_2 S_{BET} = 1687 m²/g and for Cr-MIL-101-NH_2 S_{BET} = 1850 m²/g was calculated. The micropore volume was determined at p/p_0 = 0.5. For Cr-MIL-101-NO_2 the observed micropore volume is V_m = 0.88 cm³/g, for Cr-MIL-101-NH_2 a micropore volume of V_m = 0. 96 cm³/g was determined.

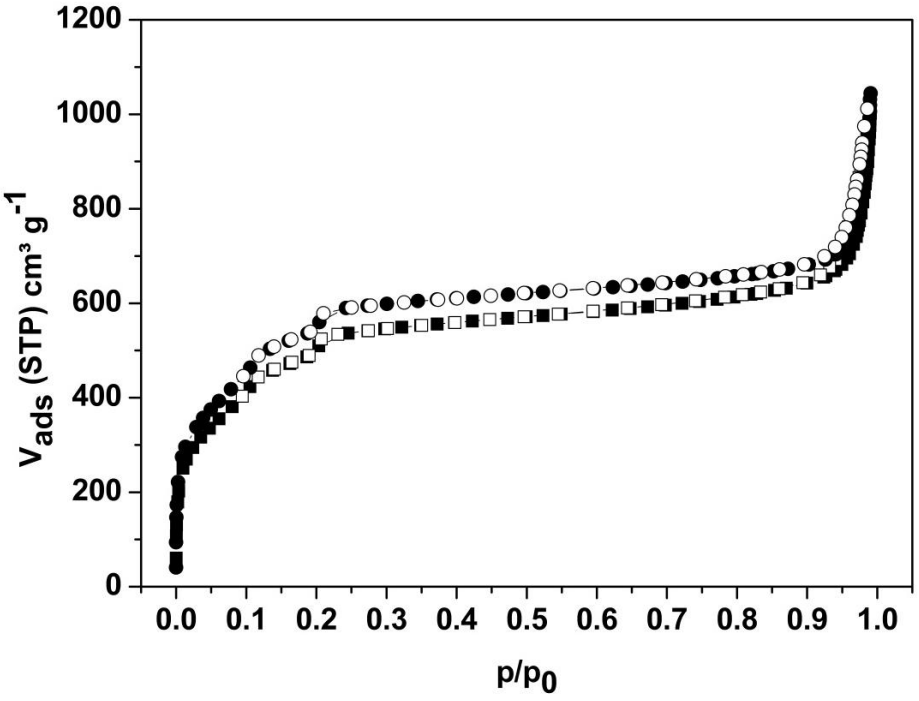

Fig. S3. N_2 adsorption isotherms of Cr-MIL-101-NO_2 (filled squares) and Cr-MIL-101-NH_2 (filled cycles) and desorption isotherm (Cr-MIL-101-NO_2 open squares, Cr-MIL-101-NH_2 open cycles).

(4) XRPD-pattern of Cr-MIL-101_amide and Cr-MIL-101_urea

The powder pattern of Cr-MIL-101_amide (Fig. S4a) indicate the intactness of the MIL structure after the post-synthetic modification reactions, since all reflections positions are the same compared to the unmodified MIL (black graph). The relative intensities are changed due to additional molecules inside the pores. Similar results are observed for Cr-MIL-101_urea (Fig. S4b).

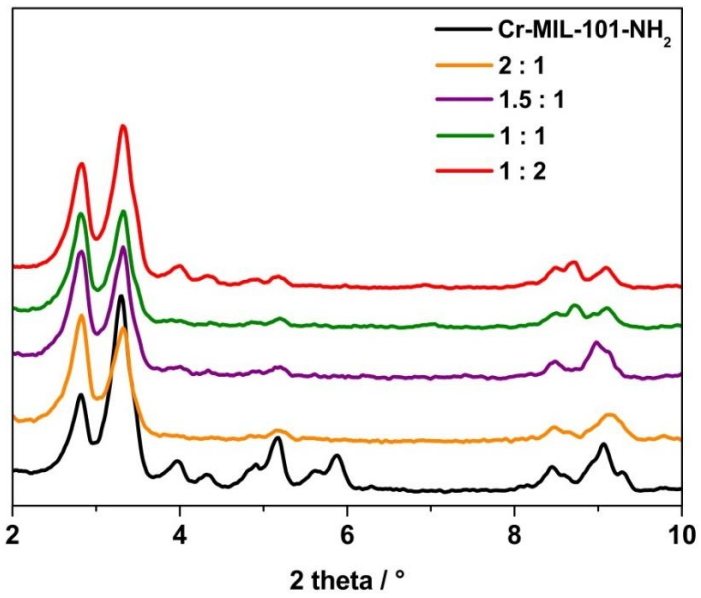

Fig. S4a. XRPD pattern of Cr-MIL-101_amide samples, synthesized with different molar ratios of MIL and dye.

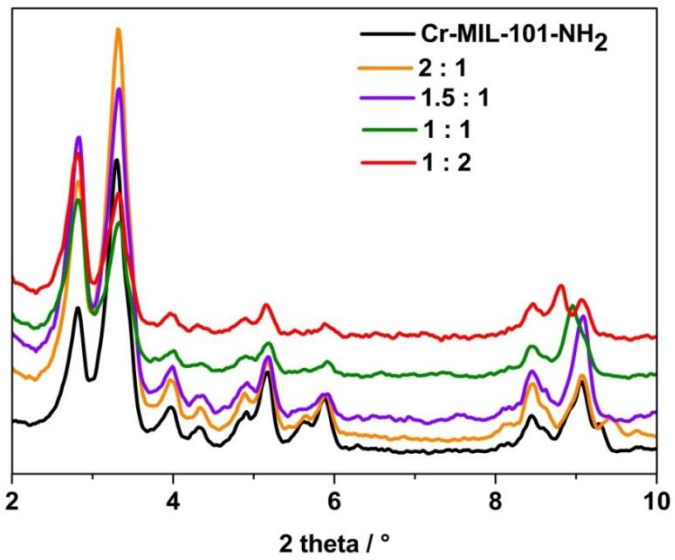

Fig. S4b. XRPD pattern of Cr-MIL-101_urea samples, synthesized with different molar ratios of MIL and dye.

(5) N_2 sorption isotherms of Cr-MIL-101_amide and Cr-MIL-101_urea

In the Figures S5a and S5b the ad- (filled squares) and desorption (open squares) isotherms of Cr-MIL-101_amide and Cr-MIL-101_urea are compared with the sorption isotherm of pure Cr-MIL-101-NH_2. In both cases the calculated surface area decreased with increasing dye concentration. This indicates that the highest switch density was achieved at the molar ratio of 1 : 2 (-NH_2 : dye). For calculated surface areas and micropore volumes see Table 1 in the main text.

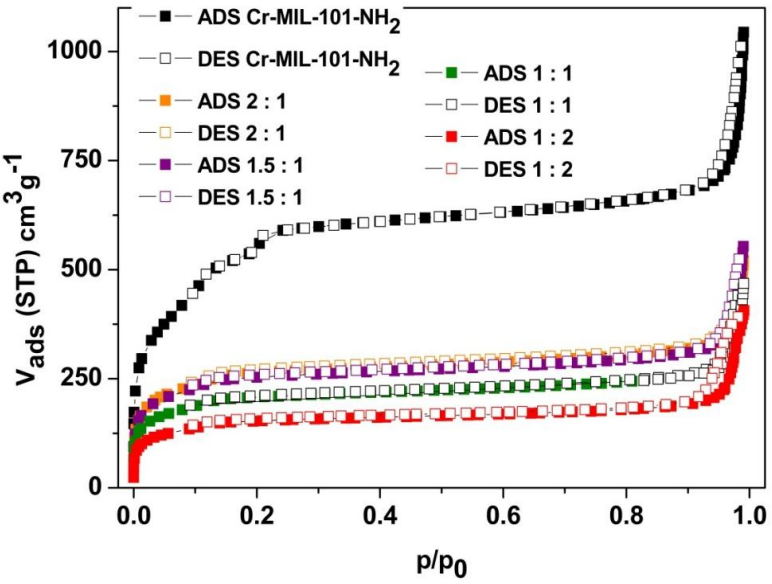

Fig. S5a. N_2 sorption isotherms of Cr-MIL-101-NH_2 (black graph) and Cr-MIL-101_amide synthesized with different molar ratios of –NH_2 : dye **1**.

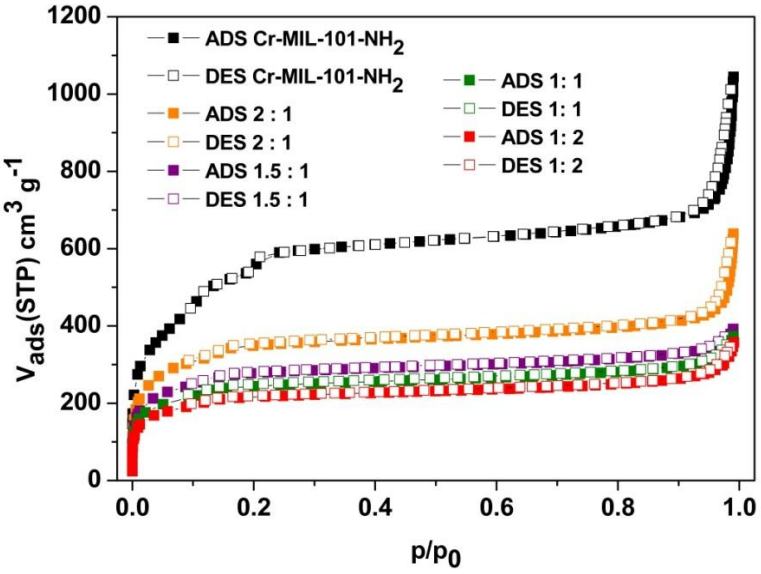

Fig. S5b. N_2 sorption isotherms of Cr-MIL-101-NH_2 (black graph) and Cr-MIL-101_urea synthesized with different molar ratios of –NH_2 : dye **2**.

(6) ^{13}CNMR- , HSQC- and COSY-spectrum of H_2-BDC_amide.

Figure S6a represents the ^{13}CNMR spectrum of H_2-BDC_amide. The signals of C-atoms are assigned to the picture as followed:

^{13}CNMR (600 MHz, DMSO-D_6): δ = 166.5 (s, *C*-1, *C*-2), 164.0 (s, *C*-3), 153.8 (s, *C*-15), 151.9 (s, *C*-16), 140.6 (s, *C*-9), 136.4 (s, *C*-10), 135.3 (s, *C*-7), 132.2 (s, *C*-21), 131.5 (s, *C*-5), 129.6 (s, C-*19*, C-*20*), 128.5 (s, C-*11*, C-*12*), 123.6 (s, C-*6*), 122.9 (s, C-*13*, C-*14*), 122.8 (s, C-*17*, C-*18*), 120.9 (s, C-*8*, C-*14*) ppm. C-*4* could not be located, which is not unusual for quaternary C-atoms.

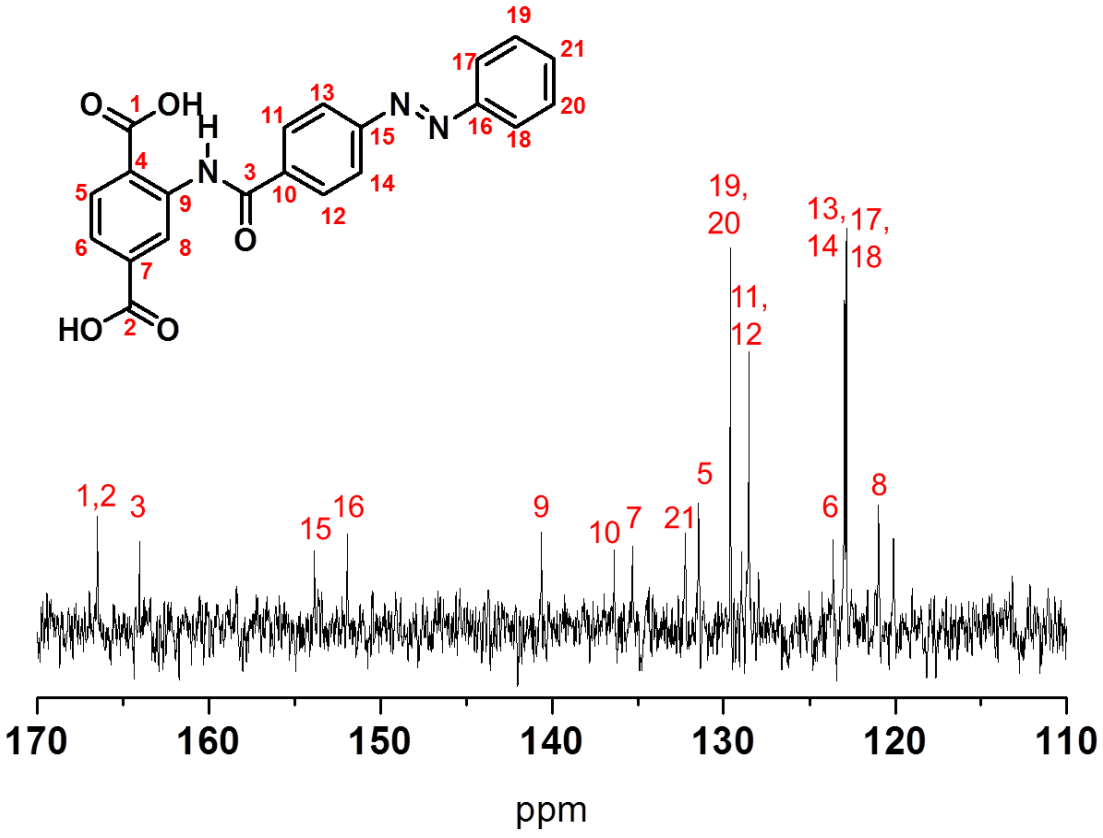

Fig. S6a. ^{13}CNMR spectrum of H_2-BDC_amide.

The ^{1}HNMR spectrum of H_2-BDC-amide was evaluated using the HSQC-spectrum (Fig. S6b) and the COSY-spectrum (Fig. S6c).

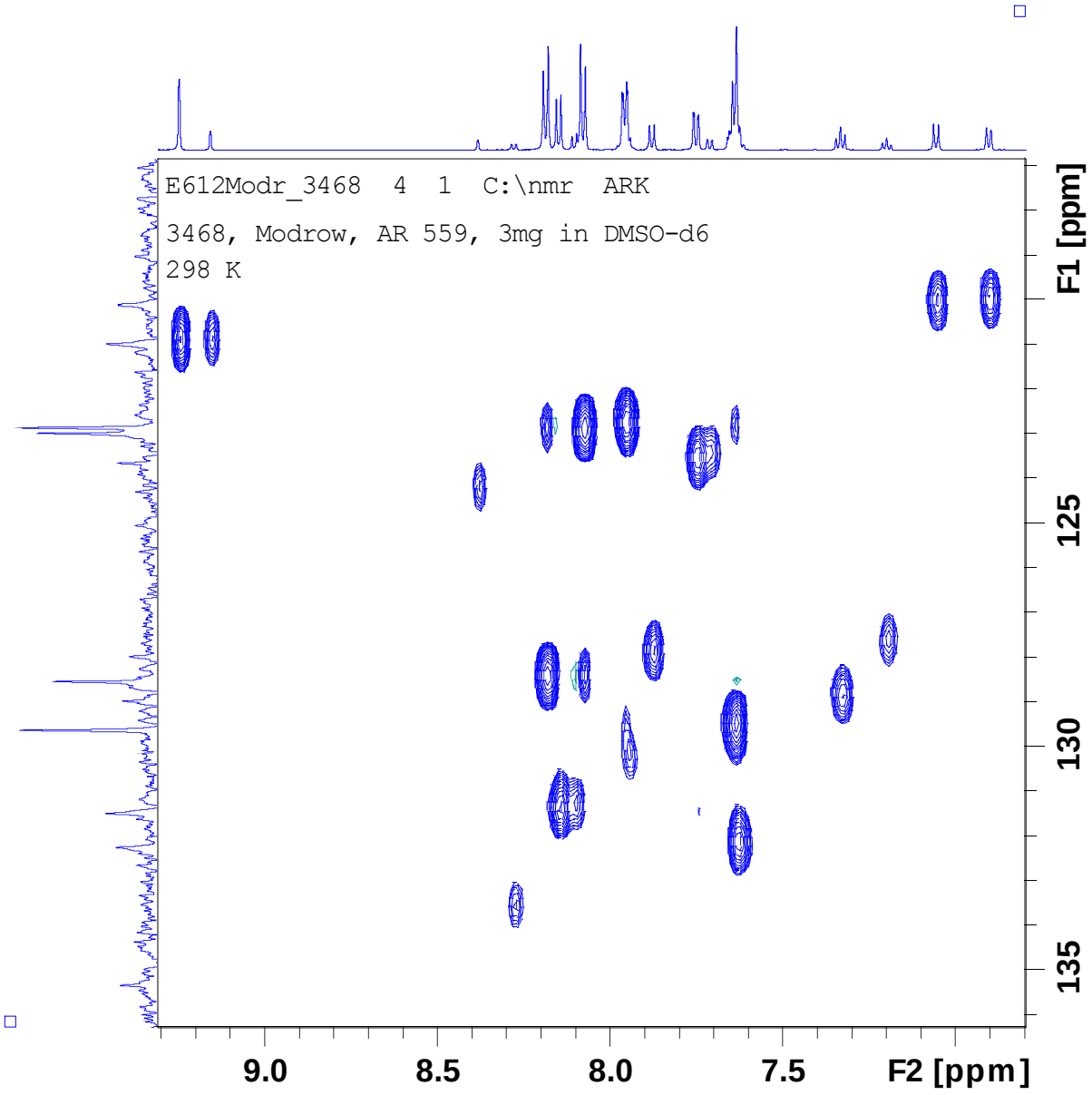

Fig. S6b. HSQC-spectrum of H_2-BDC_amide.

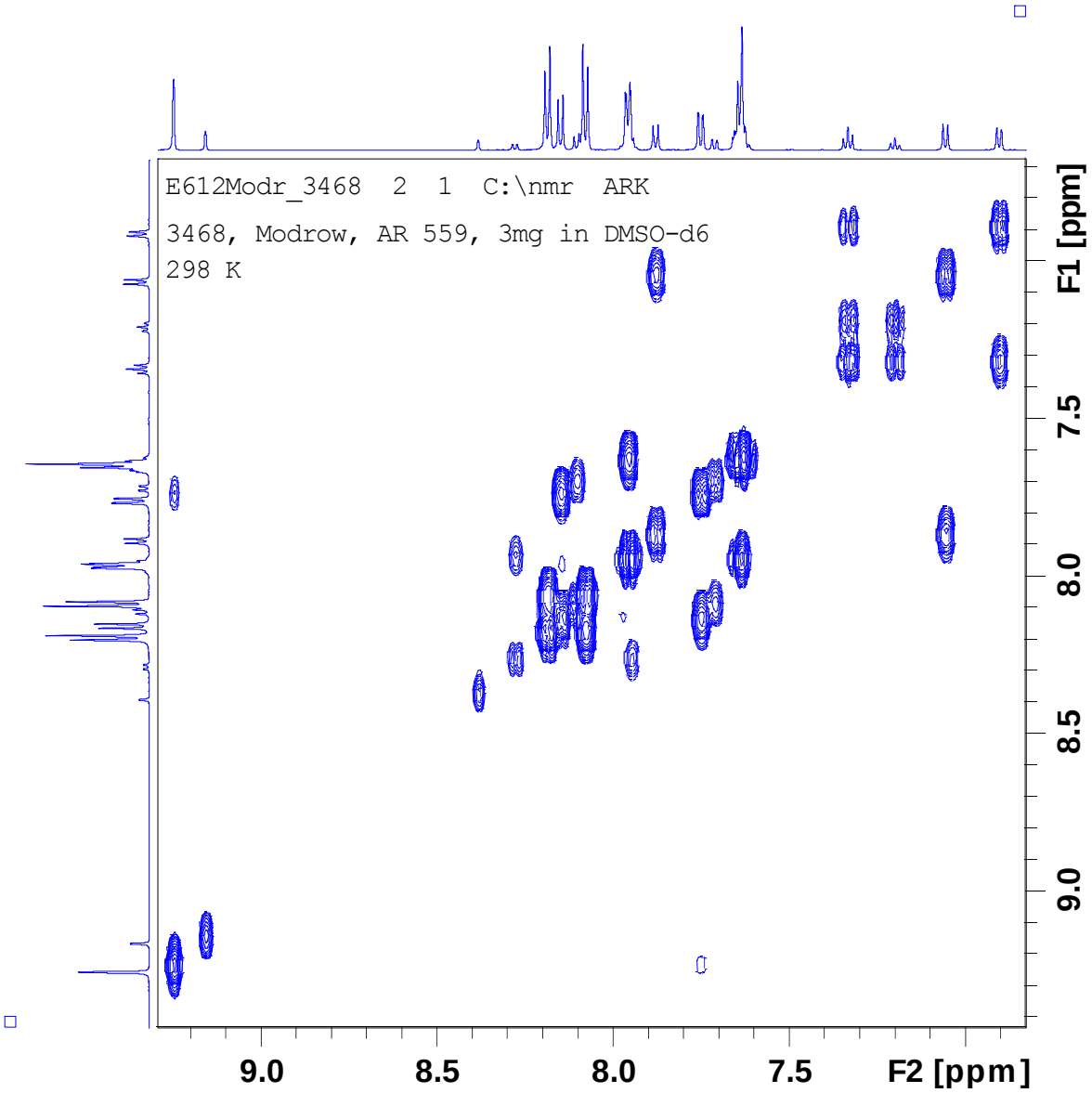

Fig. 6c. COSY-spectrum of H_2-BDC_amide.

(7) ^{13}CNMR-Dept, HMBC- and COSY- spectrum of H_2-BDC_urea

Since no quaternary carbon atoms are visible in the dept spectrum, only the aromatic carbon atoms with one hydrogen atoms could be located in the dept spectrum of H_2-BDC-urea (Fig. S7a). Here all signals of H_2-BDC_urea could be located and assigned to the molecule (numbering according to figure S7a):

^{13}CNMR-Dept (600 MHz, DMSO-D_6): δ = 131.0 (s, *C*-12), 129.1 (s, *C*-10, *C*-11), 128.8 (s, *C*-1), 123.5 (s, *C*-4, *C*-5), 122.0 (s, *C*-8, *C*-9), 120.7 (s, *C*-2), 118.4 (s, *C*-6, *C*-7)ppm.

Due to the limited solubility of H_2-BDC_urea no ^{13}CNMR could be measured.

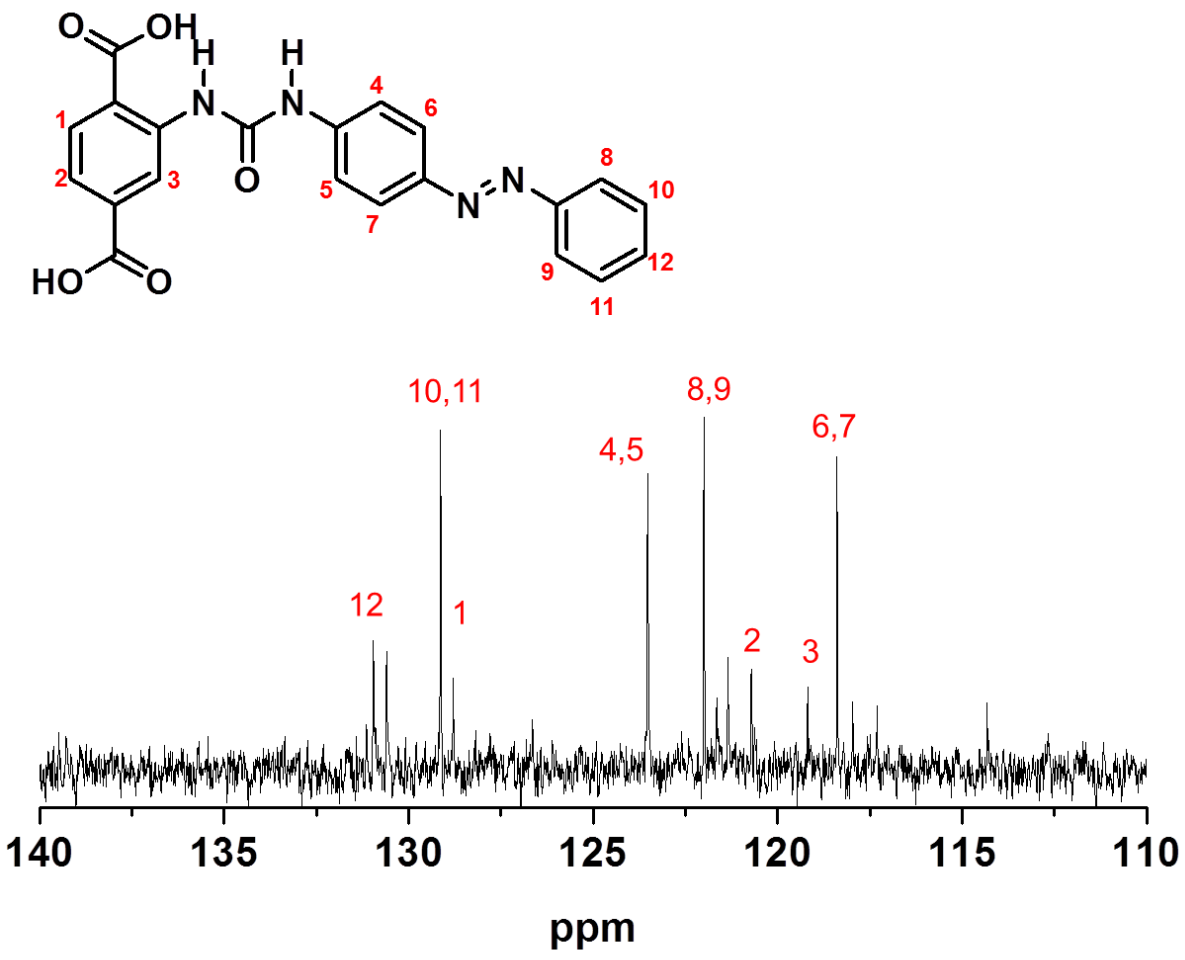

Fig. S7a. Dept ^{13}CNMR spectrum of H_2-BDC_urea.

The ^{1}HNMR spectrum of H_2-BDC_urea was evaluated using the HMBC-spectrum (Fig. S7b) and the COSY-spectrum (Fig. S7c).

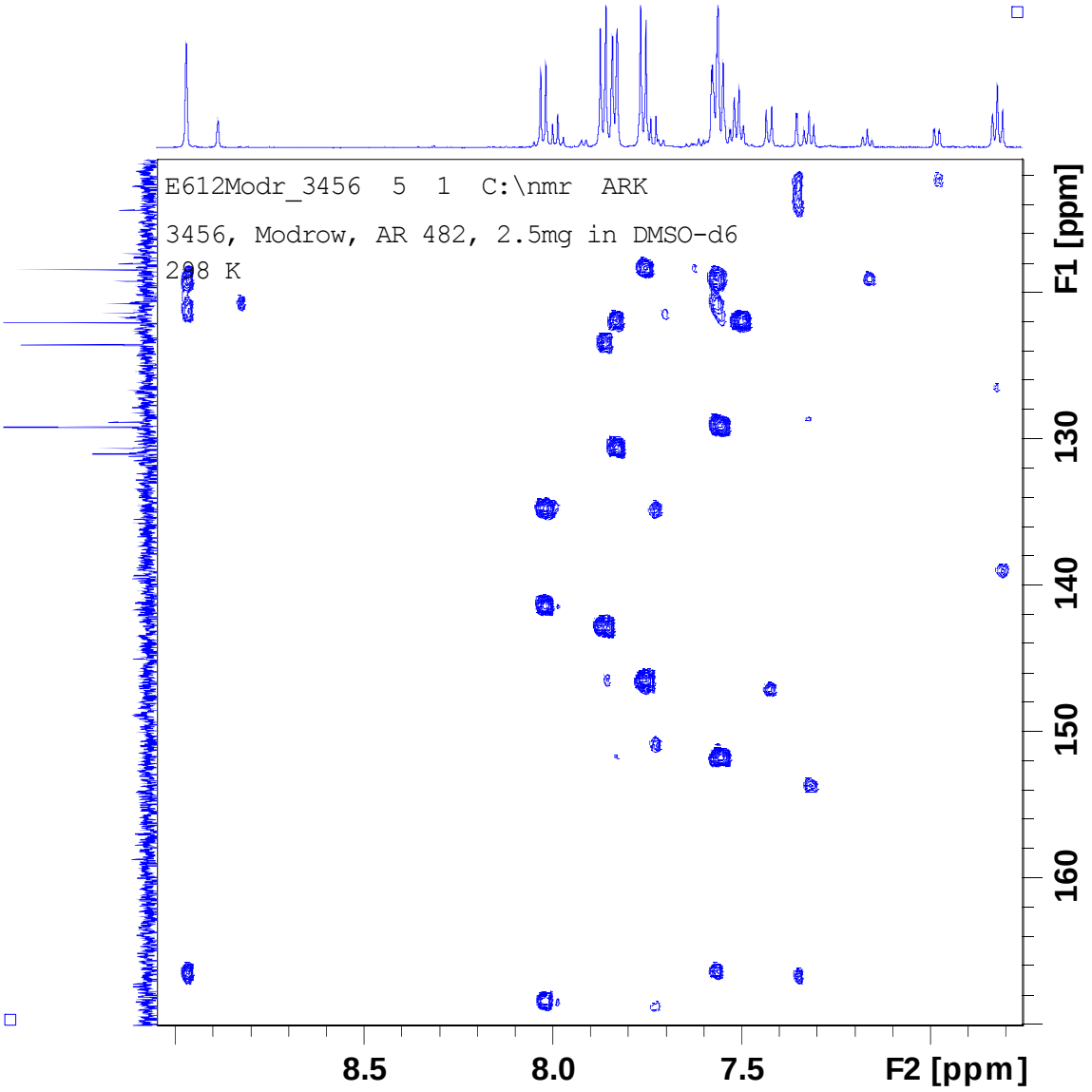

Fig. 7b. HMBC-spectrum of H_2-BDC_urea.

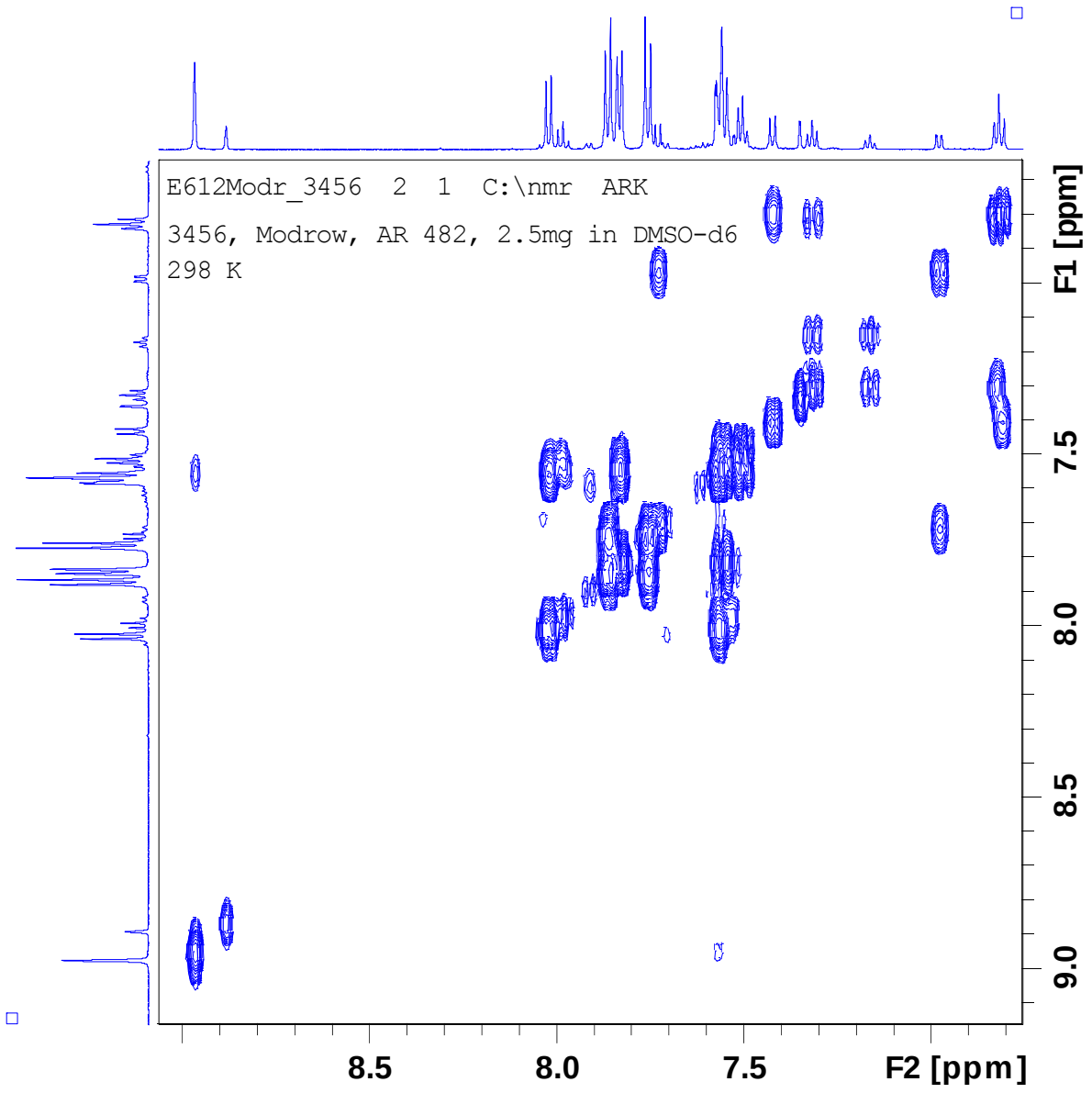

Fig. 7c. COSY-spectrum of H_2-BDC_urea.

(8) ^{1}HNMR spectra of $(H_3C)_2$-BDC_amide

In Figure S8a the ^{1}HNMR spectrum of $(H_3C)_2$-BDC_amide is shown in the region of 12 to 3.5 ppm. The signal at 11.5 ppm can be assigned to the amide proton and the prominent signal at 9 ppm could be assigned to the proton 3 (numbering according to figure S8a).

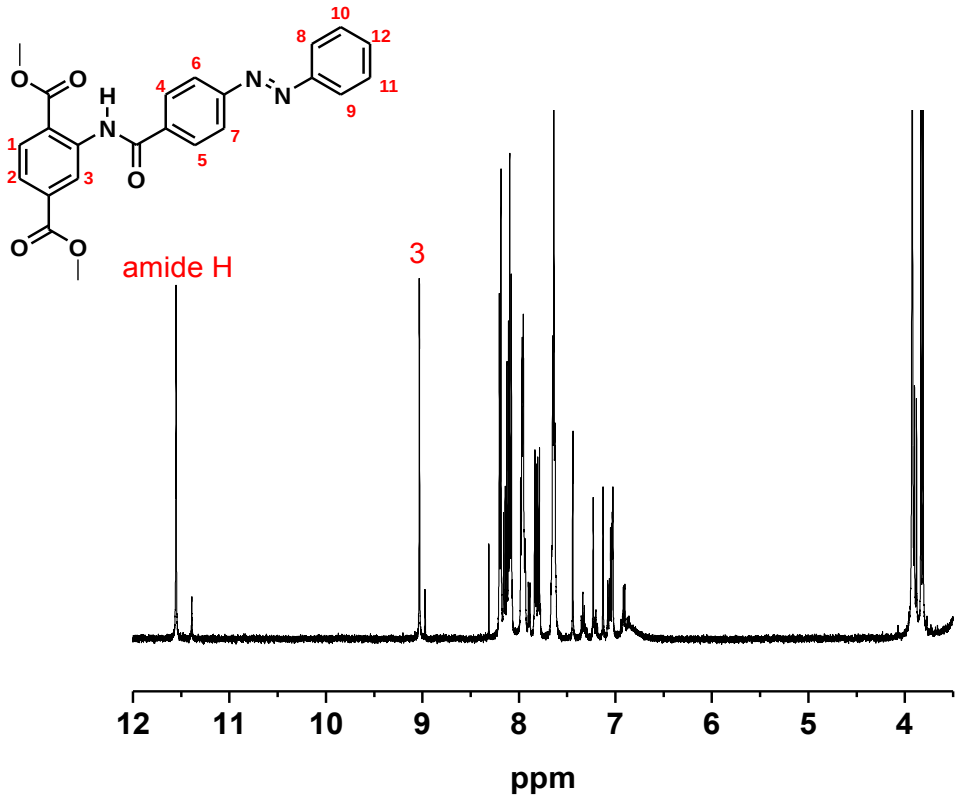

Fig. S8a. ^{1}HNMR spectrum of $(H_3C)_2$-BDC_amide in the region of 12 to 3.5 ppm.

An enlarged section (8.2 to 6.8 ppm) of the ^{1}HNMR spectrum of $(H_3C)_2$-BDC_amide is shown in Figure S8b. All protons of the desired molecule could be located in the ^{1}HNMR spectrum (numbering according to Figure S8a). The signals of the methyl groups of the dimethylester are found at 3.92 ppm, the small signal at 3.90 ppm can be assigned to the methyl groups of the other isomer. The signal at 3.8 ppm are due to the methyl groups of the aminoterephthalatedimethylester (Fig. S8c).

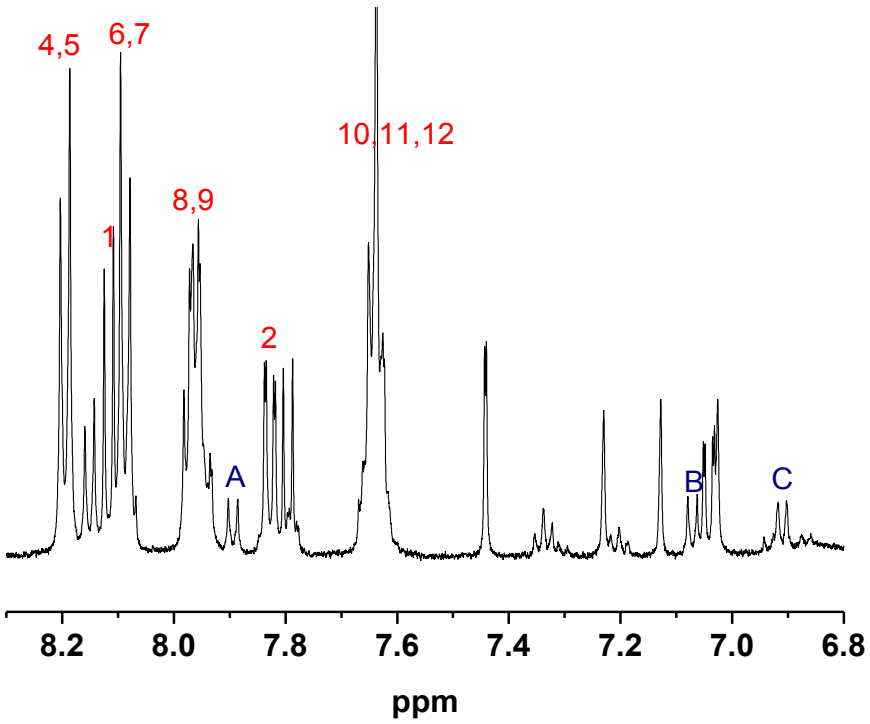

Fig. S8b. ^{1}HNMR spectrum of $(H_3C)_2$-BDC_amide in the region of 8.2 to 6.8 ppm.

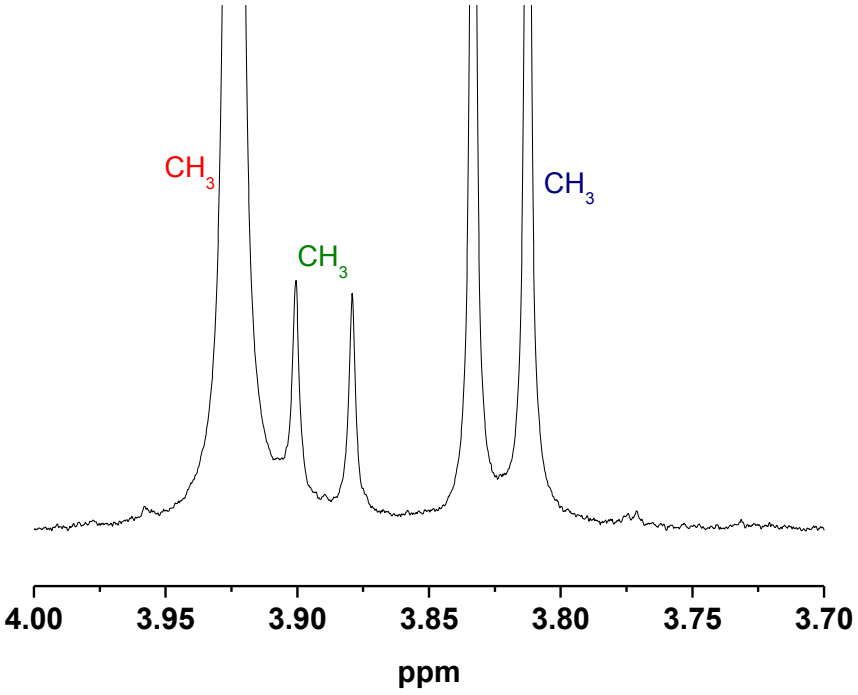

Fig. S8c. ^{1}HNMR spectrum of $(H_3C)_2$-BDC_amide in the region of 4 to 3.7 ppm.

(9) ^{1}HNMR spectra of $(H_3C)_2$-BDC_urea

Figure S9a shows the ^{1}HNMR spectrum of $(H_3C)_2$-BDC_urea in the region of 10.5 to 6.5 ppm. The signals of both urea protons are clearly visible at 10.4 and 10.2 ppm. All other protons of H_2BDC_urea could also be located and are marked in red. The protons marked in green were assigned to the other isomer of $(H_3C)_2$-BDC_urea. Since most of the signals between 7.6 and 7.0 ppm overlap, only a few protons were found. The protons of $(H_3C)_2$-BDC-NH_2 could not be located, but since the protons of the methyl groups were found (Fig. S9b), $(H_3C)_2$-BDC-NH_2 is present in the sample.

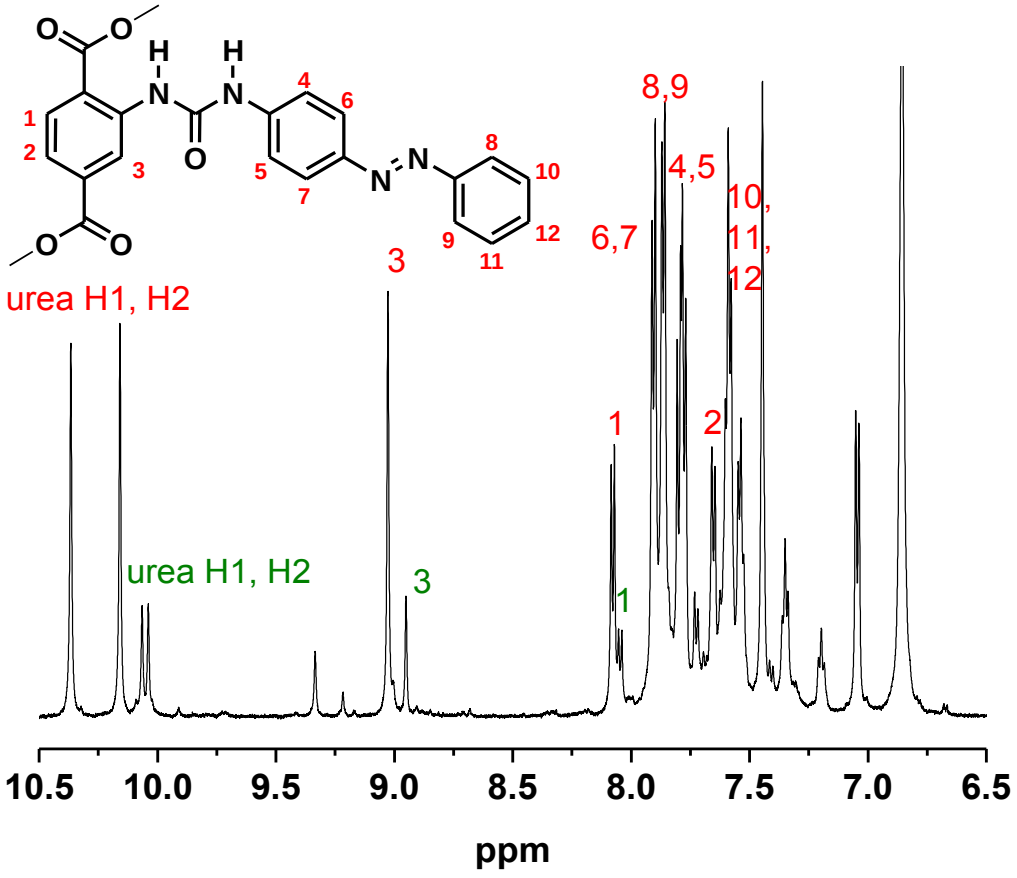

Fig. S9a. ^{1}HNMR spectrum of $(H_3C)_2$-BDC_urea in the region of 10.5 to 6.5 ppm.

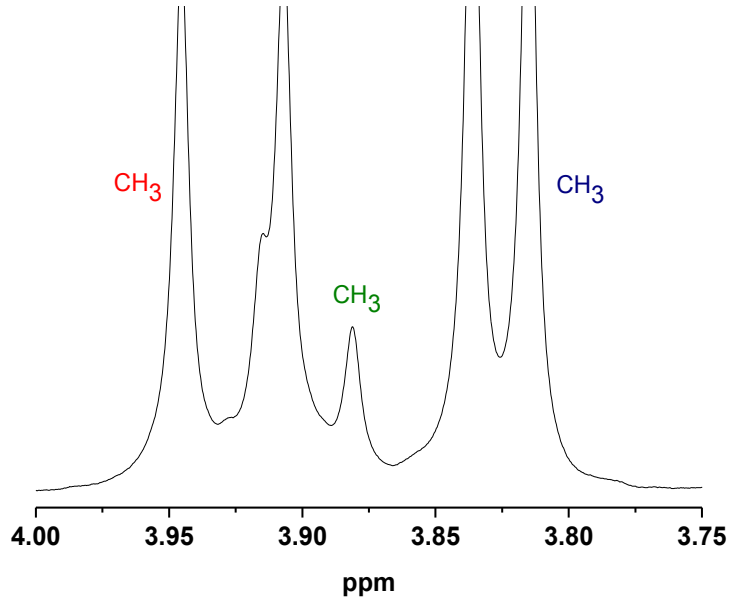

Fig. S9b. ^{1}HNMR spectrum of $(H_3C)_2$-BDC_urea in the region of 4 to 3.75 ppm.

(10) Results of the UV/Vis switching experiments of 1 and 2 in solution

Both dye molecules were dissolved in DMSO/CH_2Cl_2 before a UV/Vis spectrum was recorded (Fig. S10a, S10b). After an irradiation period of 5 min with UV light (λ = 365 nm), intensive changes are visible in the detected UV/Vis spectrum. The intensity of the π→π* transition (*trans*-isomer: 328 nm (**1**) and 332 nm (**2**), *cis*-isomer: 328 nm (**1**) and 287 nm (**2**)) decreases and the intensity of the n→π* transition (*trans*-isomer: 447 nm (**1**) and 440 nm (**2**), *cis*-isomer: 436 nm (**1**) and 437 nm (**2**)) increases. After irradiation with visible light (λ = 455 nm), the intensities changed vice versa. This process could be monitored over several switching cycles, demonstrated on the right side of the UV/Vis spectrum for the π → π* transition. Therefore, the reversible *cis/trans* isomerization of dye molecule **1** and **2** is possible in solution.

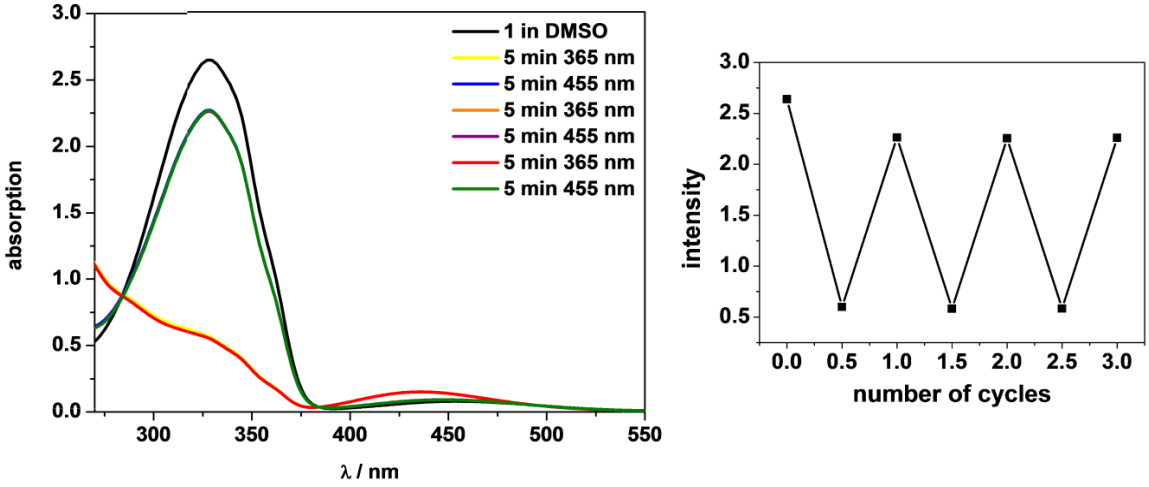

Fig. S10a: Results of the UV/Vis switching experiment of 1 in DMSO.

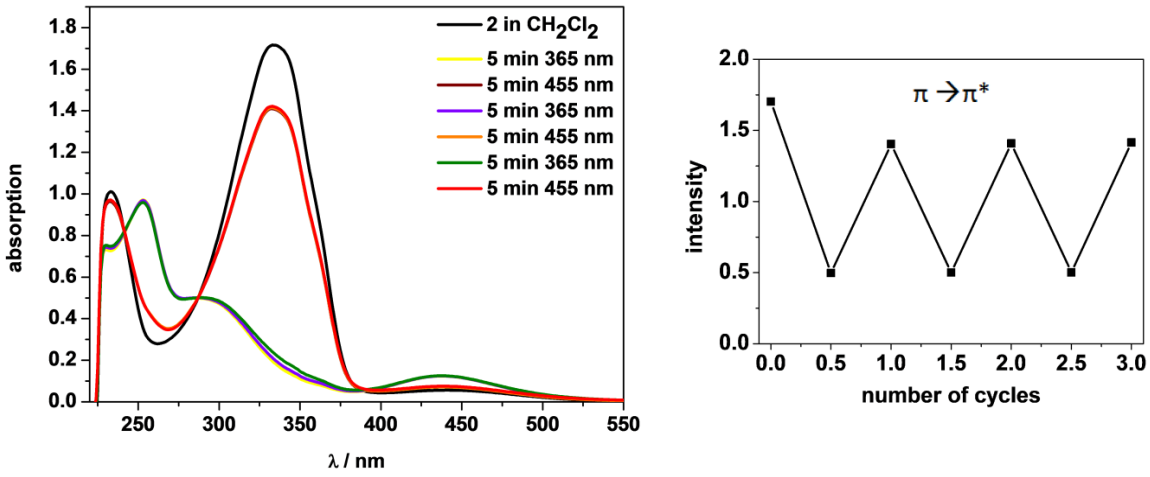

Fig. S10b: Results of the UV/Vis switching experiment of 2 in CH_2Cl_2.

(11) Results of the UV/Vis switching experiments of 1 and 2 in a $BaSO_4$ matrix

The dye molecule **1** was mixed with $BaSO_4$ and a UV/Vis spectrum was recorded (Fig. S11a). After that the sample was irradiated with UV light (λ = 365 nm) another UV/Vis spectrum was recorded (orange and purple graph, Fig. S11a). No switching effects were observed, even after the sample was irradiated with visible light (λ = 455 nm, green and red graph, Fig. S11a). This experiment indicates that the pure dye **1** does not show any switching effects in the solid state.

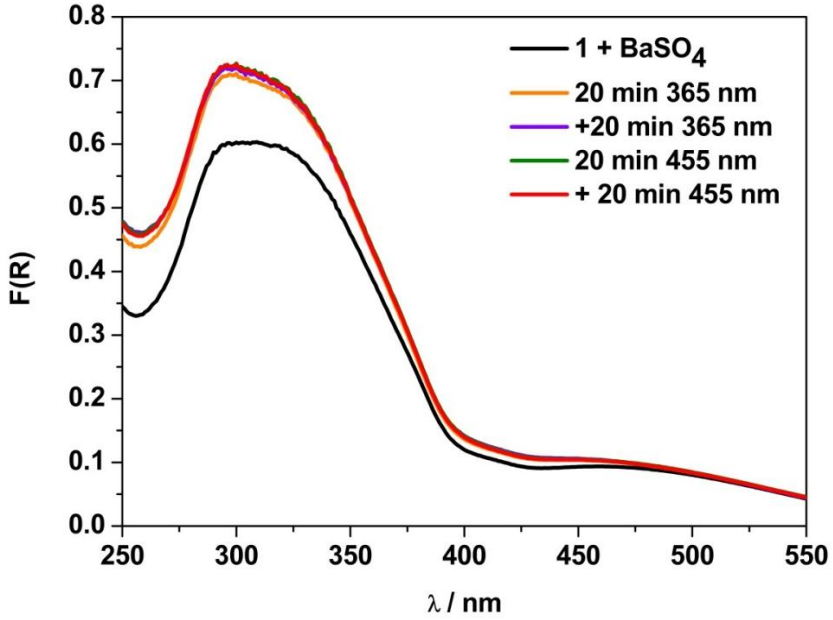

Fig. S11a. UV/Vis spectra of **1** in a $BaSO_4$ matrix.

Similar results were obtained for the UV/Vis switching experiment of the dye molecule **2** in a $BaSO_4$ (Fig. S11b). After that the sample was irradiated with UV light (λ = 365 nm), the purple and red graph (Fig. S11b) were obtained. No meaningful switching effects were observed, even after the sample was irradiated with visible light (λ = 455 nm, green graph, Fig. S11b). This experiment indicates that the pure dye **2** does not show any switching effects in the solid state.

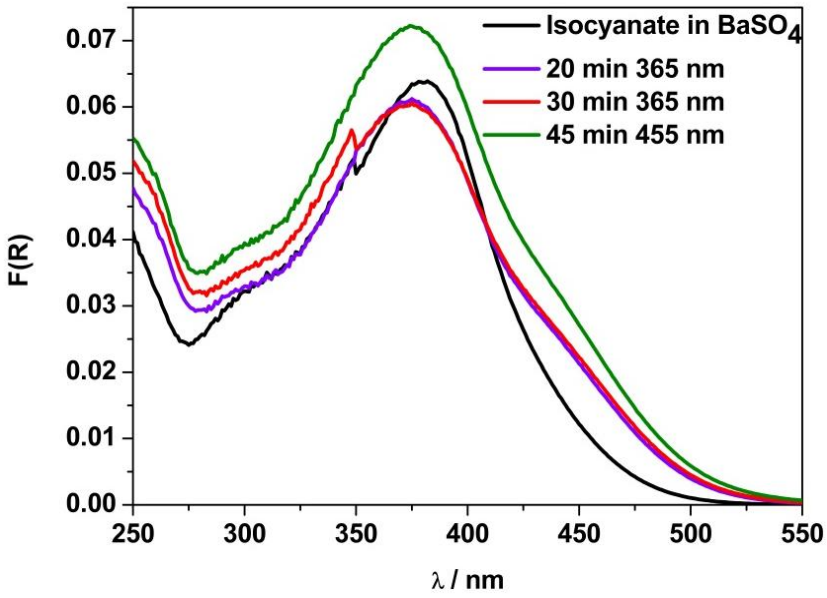

Fig. S11b: UV/Vis spectra of **2** in a $BaSO_4$ matrix.

(12) Results of the UV/Vis switching experiments of all Cr-MIL-101_amide samples

The results of all UV/Vis switching experiments of all Cr-MIL-101_amide samples are shown in Fig. 12a-d. The partial reversibility can be followed in the scheme on the right hand side of every graph. The intensities of the π →π* transition (at around 338 nm) were collected over the number of cycles.

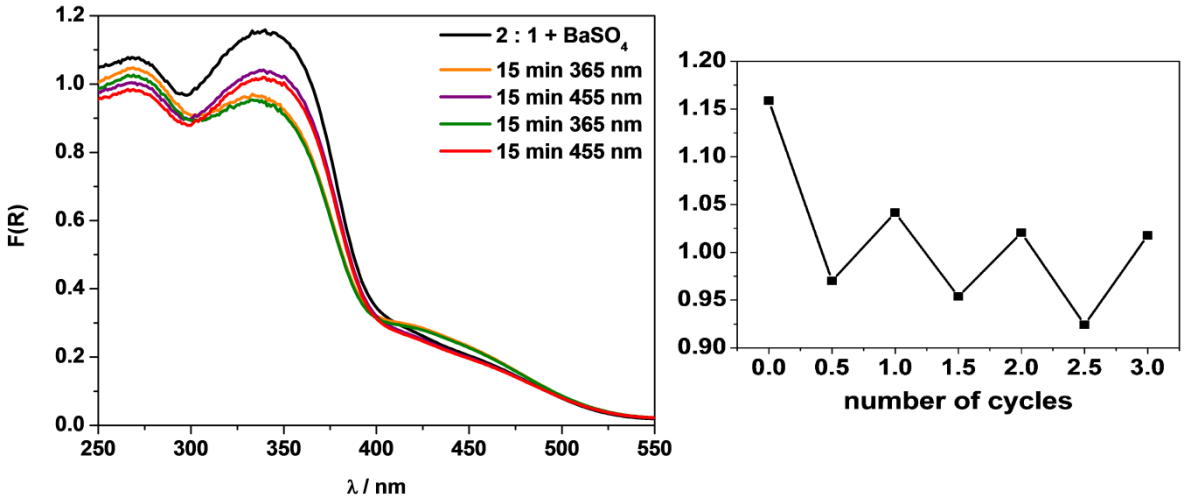

Fig. 12a. Results of the UV/Vis switching experiment of Cr-MIL-101_amide with a molar ratio of 2:1 (-NH_2 : dye).

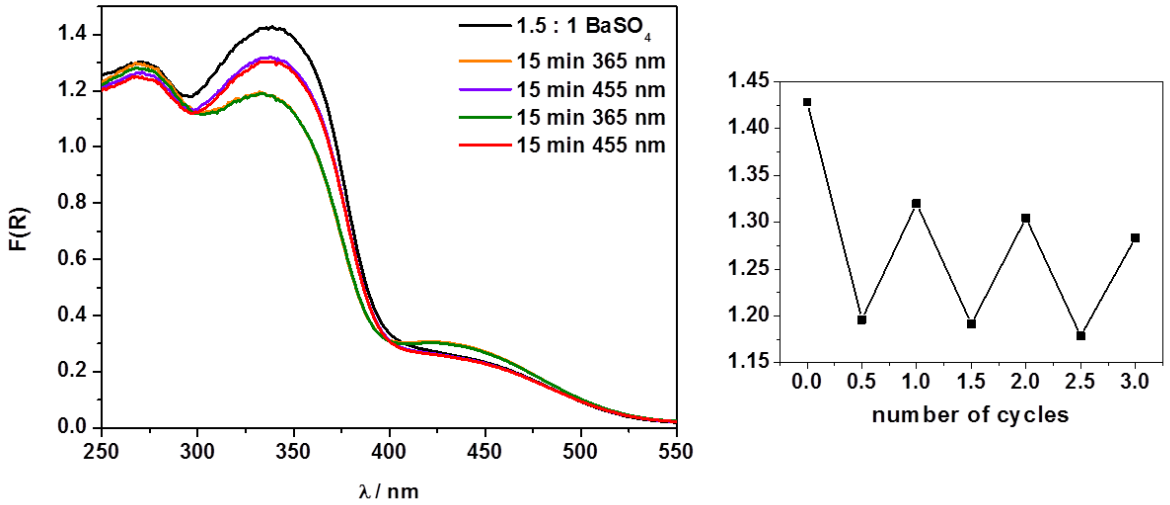

Fig. 12b. Results of the UV/Vis switching experiment of Cr-MIL-101_amide with a molar ratio of 1.5:1 (-NH_2 : dye).

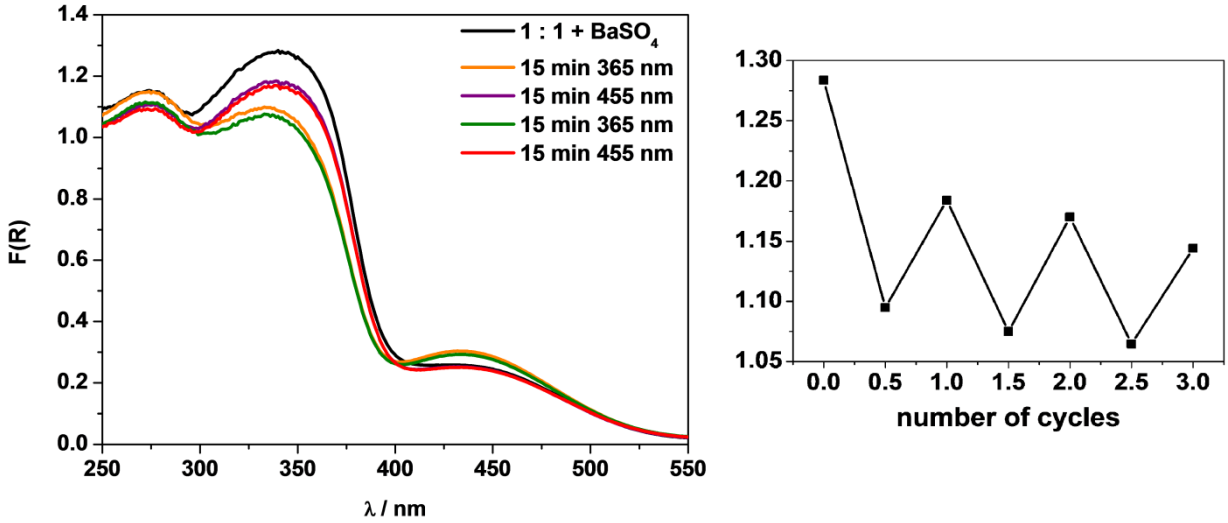

Fig. 12c. Results of the UV/Vis switching experiment of Cr-MIL-101_amide with a molar ratio of 1:1 (-NH_2 : dye).

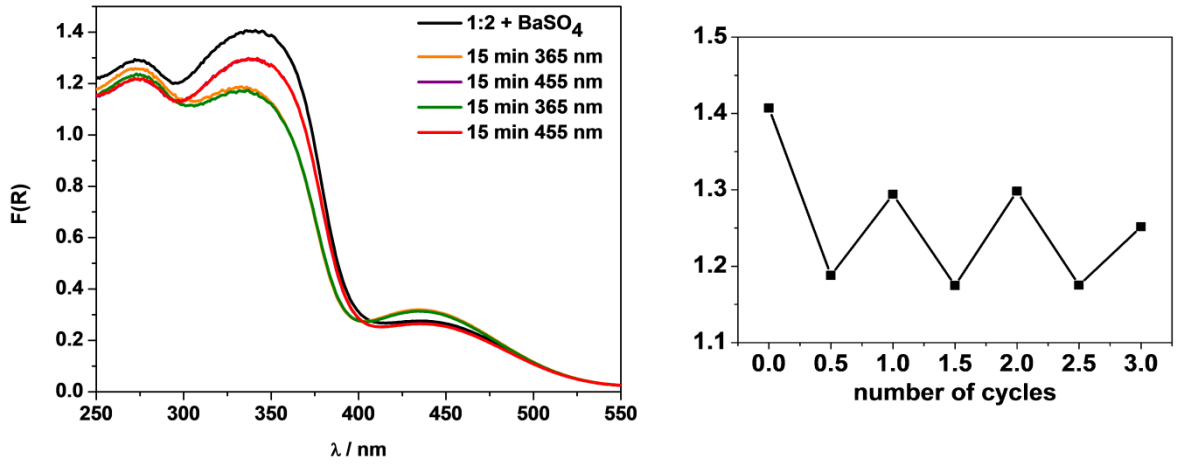

Fig. 12d. Results of the UV/Vis switching experiment of Cr-MIL-101_amide with a molar ratio of 1:2 (-NH_2 : dye).

(13) Results of the UV/Vis switching experiments of all Cr-MIL-101_urea samples

The results of all UV/Vis switching experiments of all Cr-MIL-101_urea samples are shown in Fig. 13a-d. The partial reversibility can be followed in the scheme on the right hand side of every graph. The intensities of the π →π* transition (at around 368 nm) were collected over the number of cycles.

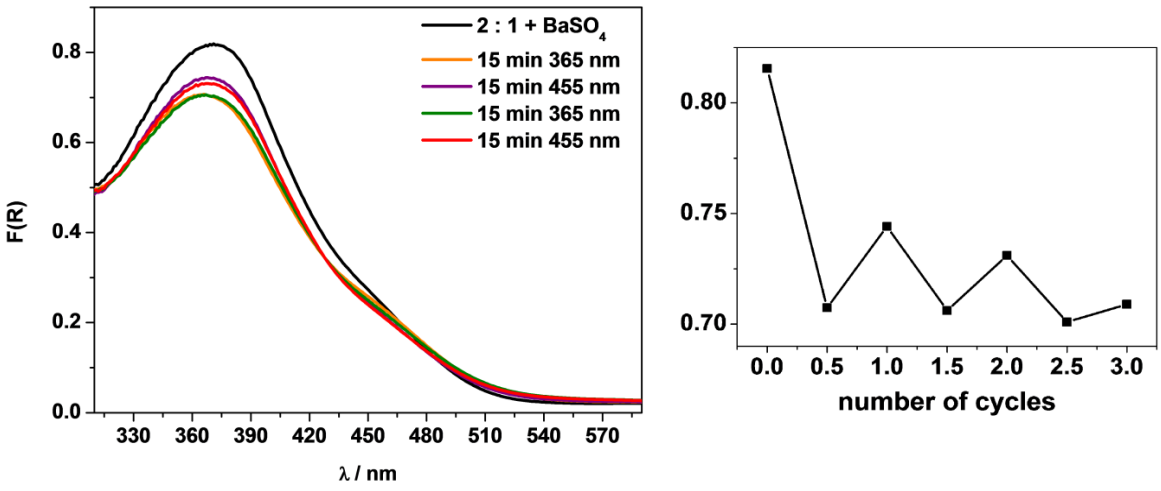

Fig. 13a: Results of the UV/Vis switching experiment of Cr-MIL-101_urea with a molar ratio of 2:1 (-NH_2 : dye) .

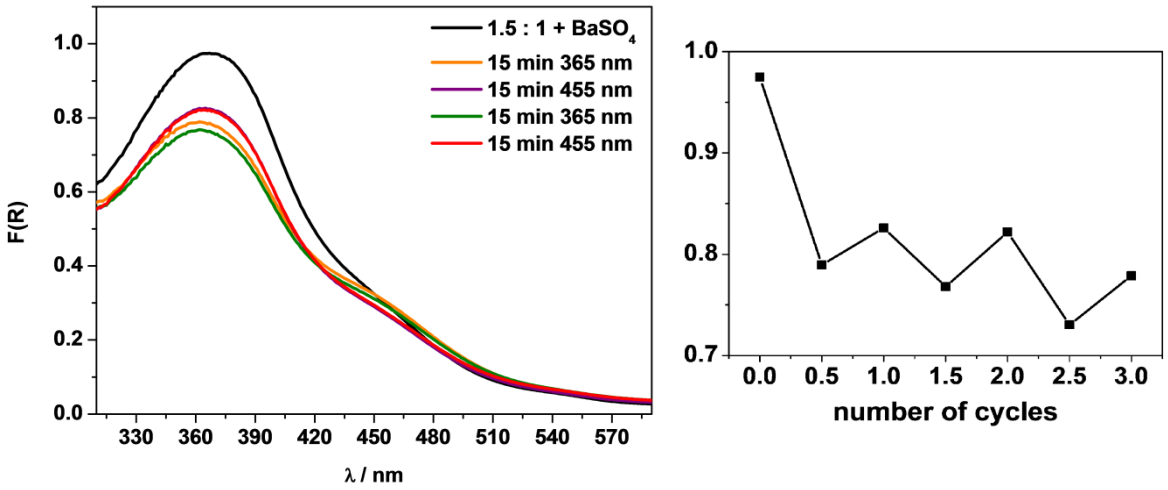

Fig. 13b: Results of the UV/Vis switching experiment of Cr-MIL-101_urea with a molar ratio of 1.5:1 (-NH_2 : dye).

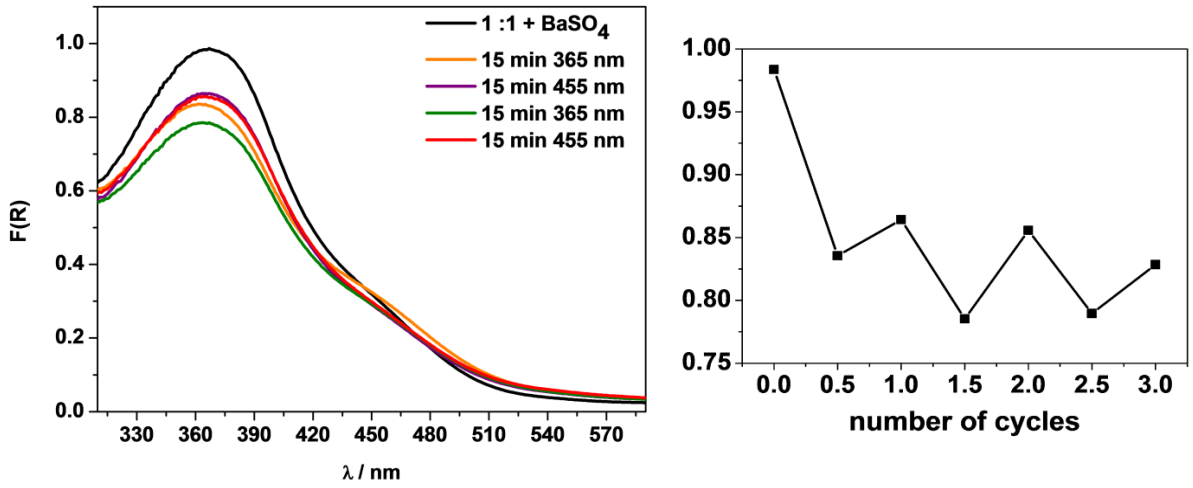

Fig. 13c: Results of the UV/Vis switching experiment of Cr-MIL-101_urea with a molar ratio of 1:1 (-NH_2 : dye).

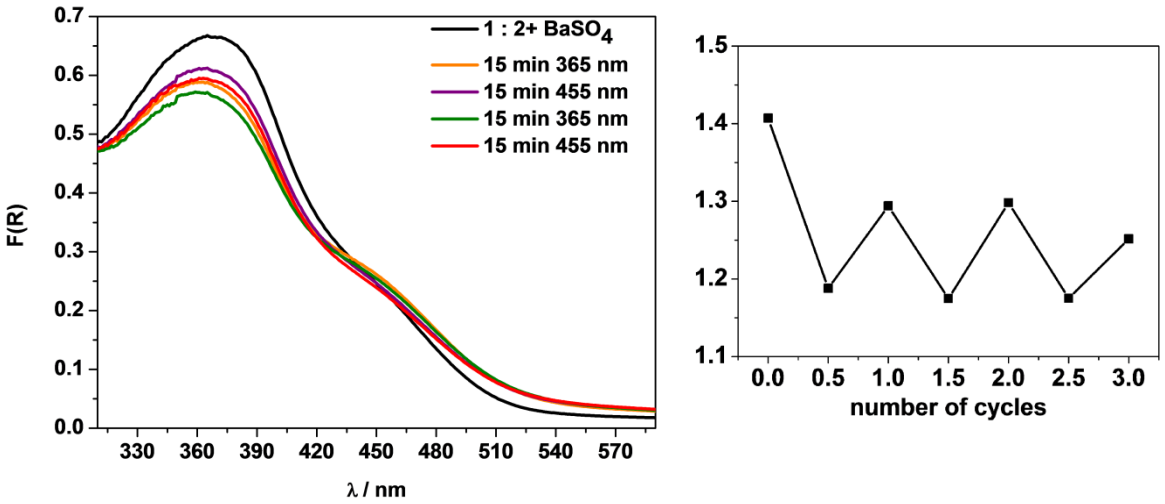

Fig. 13d: Results of the UV/Vis switching experiment of Cr-MIL-101_urea with a molar ratio of 1:2 (-NH_2 : dye).

(14) Results of the UV/Vis switching experiments of H_2-BDC_amide in DMSO

Figure S14 shows the results of the UV/Vis switching experiment of H_2-BDC_amide in DMSO. After an irradiation period of 5 min with UV light, an intensive decrease of the maxima at 337 nm is visible (red graph). The maximum increases again after irradiation with visible light (green graph). This process is reversible over several cycles (Fig. S14, right). These results proof the successful modification of Cr-MIL-101-NH_2 with **1**.

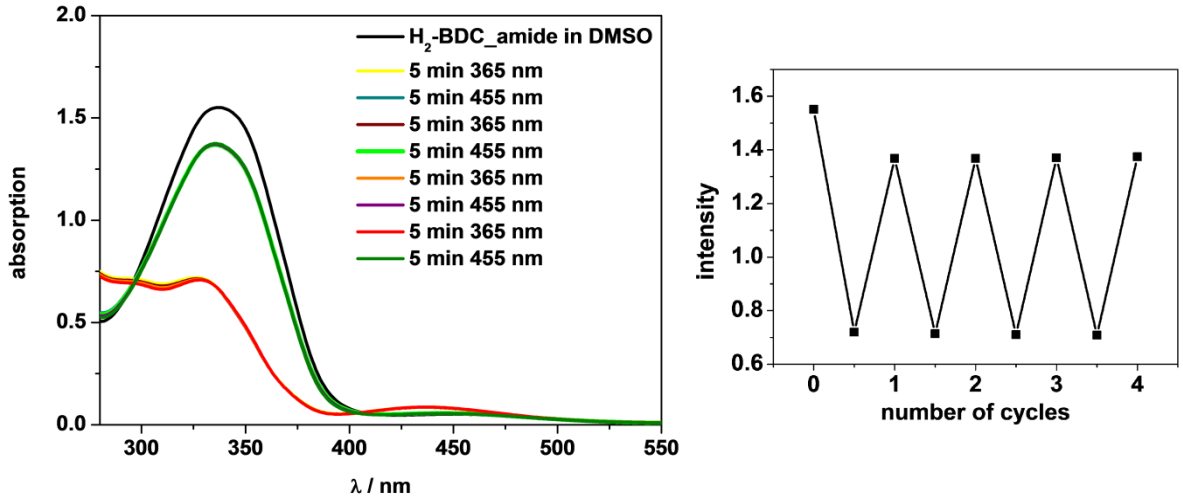

Fig. S14. Results of the UV/Vis switching experiment of H_2-BDC_amide in DMSO.

(15) Results of the UV/Vis switching experiments of H_2-BDC_urea in DMSO

Figure S15 shows the results of the UV/Vis switching experiment of H2-BDC_urea in DMSO. After an irradiation period of 5 min with UV light, an intensive decrease of the maxima at 371 nm is visible (red graph). The maximum increases again after irradiation with visible light (green graph). This process is reversible over several cycles (Fig. S15, right). These results proof the successful modification of Cr-MIL-101-NH_2 with **2**.

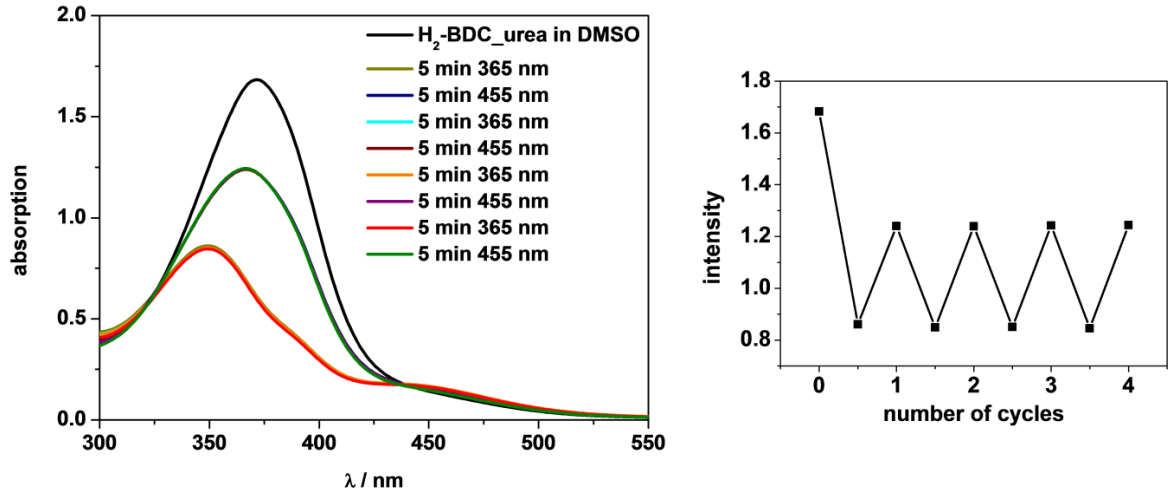

Fig. S15: Results of the UV/Vis switching experiment of H_2-BDC_urea in DMSO.

(16) Results of the thermal relaxation of Cr-MIL-101_amide

Figure S16 shows the results of the thermal relaxation of Cr-MIL-101_amide. The intensity of the π→π* band decreased after an irradiation period of 15 min with UV light and the maximum of the n→π* transition band increased (Fig. S16, green graph). After 16 h at room temperature (sample was left in the dark) no changes were observed in the UV/Vis spectrum of Cr-MIL-101_amide (Fig. S16, red graph).

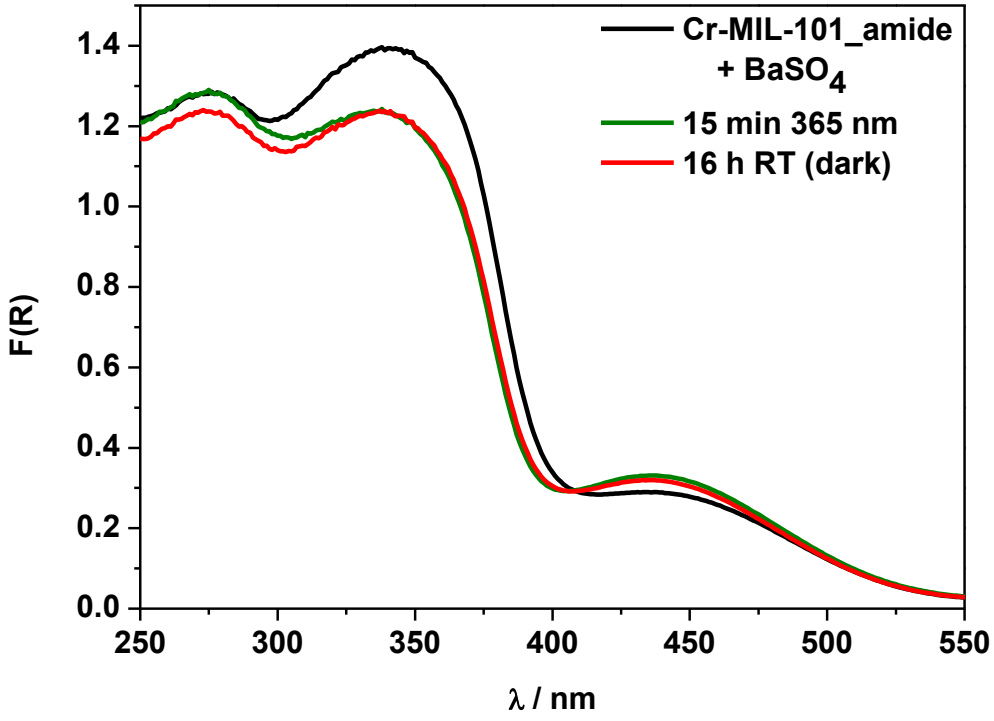

Fig. S16. Results of the thermal relaxation of Cr-MIL-101_amide.

(17) Results of the thermal relaxation of Cr-MIL-101_urea

Figure S17 shows the results of the thermal relaxation of Cr-MIL-101_urea. The intensity of the π→π* band decreased after an irradiation period of 15 min with UV light (Fig. S17, green graph). After 16 h at room temperature (sample was left in the dark) only small changes were observed in the UV/Vis spectrum of Cr-MIL-101_urea (Fig. S17, red graph).

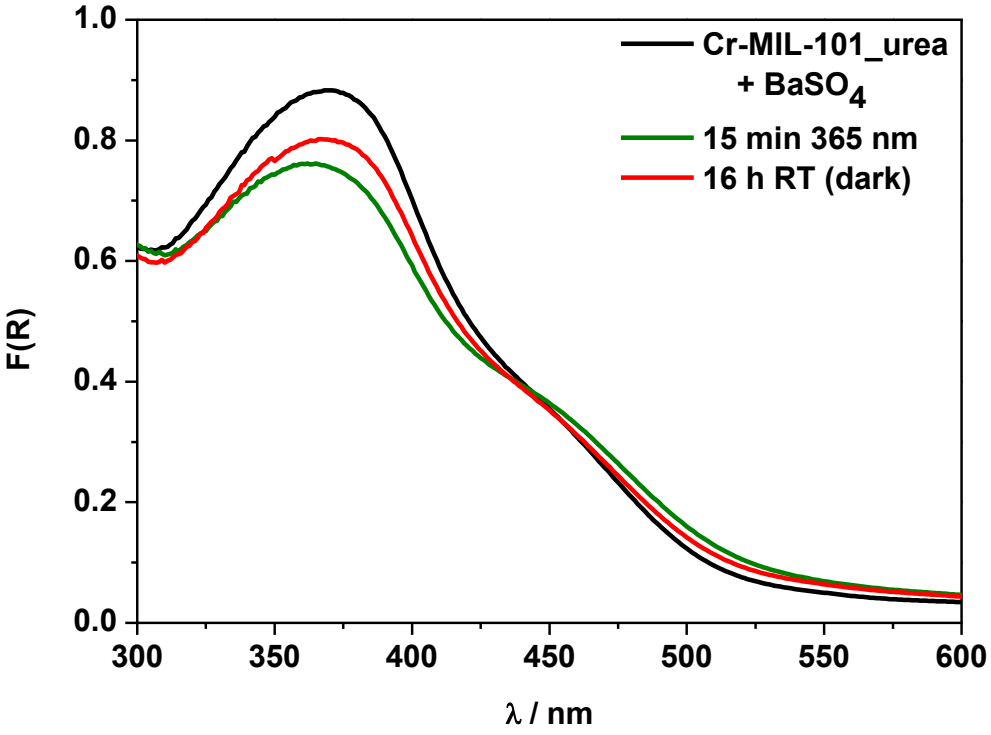

Fig. S17. Results of the thermal relaxation of Cr-MIL-101_amide.